Article



http://pubs.acs.org/journal/acsodf

# Nickel-Functionalized Nanoporous Heterostructure Microparticles for Immunoglobulin G Adsorption and Separation with High **Efficiency**

Yang Zhang, Wanting Zhang, Iin Li, Jiaxin Han, Xiangyang Gong, and Mengmeng Wang\*



Cite This: ACS Omega 2025, 10, 35187-35195



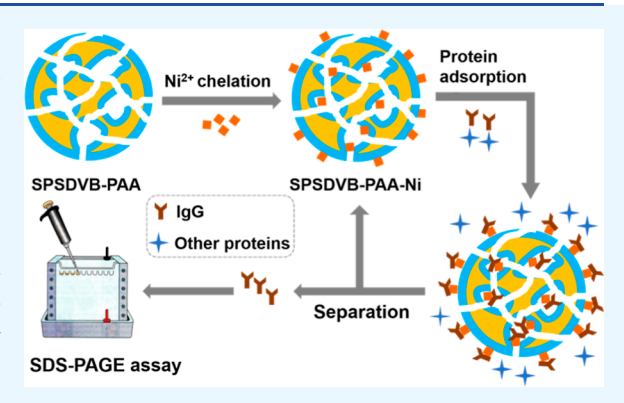
ACCESS I

Metrics & More

Article Recommendations

s Supporting Information

ABSTRACT: Developing advanced affinity adsorbents for immunoglobulin G (IgG) selective separation and purification is vital for clinical diagnosis and therapy. However, high-cost and low-specificity methods hinder high-purity IgG production. This work has fabricated nanoporous heterostructure microparticles by emulsion polymerization of styrene, divinylbenzene, and acrylic acid on the surface of sulfonated polystyrene particles. Following modification with nickel ions, the Ni<sup>2+</sup>-functionalized sulfonated poly(styrene-divinylbenzene)-poly(acrylic acid) (SPSDVB-PAA-Ni) exhibits dense nanoporous heterostructures and Ni<sup>2+</sup>-chelating sites, enabling electrostatic attraction and metal affinity interactions for the adsorption and separation of IgG. The SPSDVB-PAA-Ni affinity adsorbent demonstrates a high adsorption capacity of 192.7 mg·g<sup>-1</sup> with rapid equilibration within 30 min, outperforming protein A/G



adsorbents. Furthermore, the separation/purification of IgG from human serum samples is successfully achieved with a recovery of 73.7% and a purity of 83.7%. The study presents the SPSDVB-PAA-Ni polymer microparticles as promising adsorbents for selectively separating antibody drugs, suggesting their potential applications in clinical analysis.

### 1. INTRODUCTION

Immunoglobulins (Ig), a class of antibodies produced by B lymphocytes, are categorized into five types: IgE, IgD, IgA, IgM, and IgG. 1,2 Among them, IgG constitutes the highest antibody content in immunoglobulins and is widely distributed in human tissues and plasma.<sup>3,4</sup> IgG antibodies play a crucial role in preventing transplant rejection, combating viral and bacterial infections, and managing inflammatory and autoimmune diseases. 5,6 For instance, plasma IgG aggregates could be applied as biomarkers in the diagnosis, prognostic assessment, and therapeutic monitoring of multiple sclerosis. Tumor cell-derived IgG plays a major role in tumor development, including promotion of growth, invasion, and metastasis, and may serve as therapeutic targets and prognostic markers.8 Hence, the development of an IgG separation method is crucial for the production of biopharmaceuticals.

The separation/purification approaches of IgG include precipitation, affinity chromatography, io ion-exchange chromatography, 11 and hydrophobic interaction chromatography. 12 Therein, affinity chromatography is the most useful method for capturing and purifying IgG due to its utilization of proteins A, G, and L as natural affinity ligands, which have a strong affinity for the fragments of IgG. 13,14 However, these ligands suffer from high cost, instability, leakage, and degradation. 15,16 In recent years, several abiotic ligands with low cost, chemical stability, and high selectivity have been developed as

substitutes for IgG purification, including biomimetic protein G, thiophilic ligands, and immobilized metal ions.

Immobilized metal-ion affinity chromatography (IMAC) has gained widespread acceptance in separating proteins, peptides, nucleic acids, and enzymes with the advantages of high capacity, high selectivity, and low cost. 18,19 IMAC utilizes transition metal ions immobilized on a solid matrix as ligands because of their affinity for electron-donating amino acid residues, such as histidine, cysteine, and tryptophan.<sup>20</sup> Owing to the metal affinity interaction between Ni2+ and histidine residues, Ni<sup>2+</sup>-based affinity adsorbents are commonly used for the purification of histidine-rich proteins or His-tagged proteins. 21-24 Limited research has been conducted on the purification of IgG using Ni<sup>2+</sup>-based affinity adsorbents. For example, Todorova-Balvay et al. discovered, through molecular modeling, that the Fc domain of IgG contains a cluster of histidine residues that are accessible and capable of binding to transition metal ion chelates, while it was only theoretical research. 25 Mourao et al. found that chelating Ni<sup>2+</sup>, Cu<sup>2+</sup>, Co<sup>2+</sup>,

Received: May 23, 2025 Revised: July 2, 2025 Accepted: July 29, 2025 Published: August 1, 2025





and Zn<sup>2+</sup> with CM-Asp-agarose showed potential in isolating Fab fragments from papain-digested human IgG with high selectivity and good separation efficiency. However, Nichelated CM-Asp-agarose was applied in the purification of Fab fragments from digested human IgG, not intact IgG. Therefore, our work has developed Ni<sup>2+</sup>-immobilized affinity adsorbents for IgG purification for the first time, expanding the application scope of the adsorbent.

Polymer microparticles are frequently used as separation materials for removing pollutants from water, purifying proteins from matrixes, and identifying biomarkers in biofluids.<sup>27,28</sup> These polymer microparticles include homogeneous nanoporous silica, molecularly imprinted polymers (MIPs), metal-organic frameworks (MOFs), block copolymers, and heterostructure microparticles.<sup>29</sup> Among them, the heterostructure microparticles fabricated through emulsion interfacial polymerization have allowed for the efficient isolation of complex biosamples. This is due to their diverse pore structure, tunable surface groups, and pore sizes. 30,31 For example, Song et al. synthesized heterostructure-enabled separation particles (HESPs) for rapid separation of similarly sized proteins, mainly relying on electrostatic interaction.<sup>32</sup> To improve selectivity and capacity in separation, surface modification with specific groups is in demand. Wang et al. fabricated macroporous polymer microspheres that were subsequently modified with polyethylenimine and P<sub>5</sub>W<sub>30</sub> through electrostatic interaction.<sup>33</sup> SPSDVB-PAA-PEI-P<sub>5</sub>W<sub>30</sub> exhibited excellent adsorption selectivity for glycoproteins. Nevertheless, the problems of low adsorption capacity and tedious modification methods still exist. Therefore, there is a growing need to create appropriate surface-functionalized polymer microparticles with prominent separation capability.

In this study, heterostructure poly(styrene-divinylbenzene)-poly(acrylic acid) microparticles with a nanoporous structure were fabricated and followed by immobilization with Ni<sup>2+</sup> via electrostatic interaction. The polymer microparticles, named SPSDVB-PAA-Ni, are assessed as solid-phase adsorbents in capturing and purifying IgG. Attributed to metal coordination interaction and electrostatic interactions, SPSDVB-PAA-Ni demonstrates favorable selectivity and adsorption capacity for IgG, which is utilized to separate IgG from human serum samples via SDS-PAGE. Consequently, a novel approach for purifying antibodies has been developed with potential applications in the biological medicine field.

### 2. EXPERIMENTAL SECTION

**2.1. Chemicals and Materials.** Nickel sulfate hexahydrate (NiSO<sub>4</sub>·6H<sub>2</sub>O) and poly(vinyl alcohol) were supplied by Aladdin Biochemical Technology Co., Ltd. Styrene, bovine serum albumin (BSA), polyvinylpyrrolidone, and transferrin (Trf) were obtained by Sigma-Aldrich (St. Louis, USA). 2,2'-Azoisobutyronitrile was purchased from Shanghai Sihewei Chemical Co., Ltd. Divinylbenzene, with a concentration of 80%, was sourced from Macklin Biochemical Co., Ltd. Sodium dodecyl sulfate (SDS), acrylic acid, tris(hydroxymethyl) aminomethane (Tris), cetyltrimethylammonium bromide (CTAB), imidazole, and Coomassie brilliant blue were supplied by Sinopharm Chemical Reagent Co., Ltd. 1-Chlorodecane was acquired by J&K Scientific Co., Ltd. Hydrochloric acid, acetic acid, phosphoric acid, boracic acid, sodium hydroxide, and ethanol were supplied by Tianjin Damao Chemical Co., Ltd. IgG was obtained from Yuan Ye Biotechnology Co., Ltd. The reagents mentioned above were

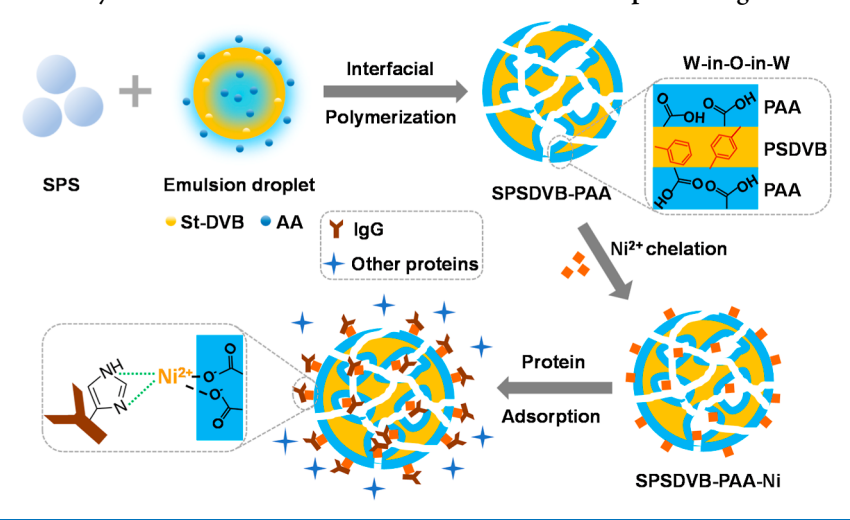
all of analytical grade, and deionized water was utilized for the entire experiment. The human serum samples were donated by the Second Affiliated Hospital of Shenyang Medical College.

- **2.2.** Instrumentations. The microstructure of SPSDVB-PAA-Ni was recorded by HITACHI SU8010 scanning electron microscopy (SEM). The cross-sectional microscopic morphologies of SPSDVB-PAA-Ni particles were observed using JEM-1200 EX transmission electron microscopy (TEM). Functional groups of SPSDVB-PAA-Ni were measured using a Fourier transform infrared (FTIR) spectrometer (FTIR-850). The X-ray photoelectron spectroscopy (XPS) analysis carried out on a Thermo ESCALAB 250Xi provided the chemical structure of SPSDVB-PAA-Ni. The nitrogen adsorption/desorption tests were conducted by using a Micromeritics ASAP TriStar II 3020 system. The zeta potentials of SPSDVB-PAA-Ni were measured by using a BT-Zeta100 analyzer. The absorbance of the protein solution was determined by utilizing a Beijing Puxi General T6 UV—vis spectrophotometer.
- **2.3. Synthesis of SPSDVB-PAA-Ni.** The procedures for preparing sulfonated polystyrene (SPS) and sulfonated polystyrene-divinylbenzene)-poly(acrylic acid) (SPSDVB-PAA) microparticles are described in Supporting Information. SPSDVB-PAA-Ni was synthesized as follows: SPSDVB-PAA (0.1 g) microparticles were dissolved in 50 mL of water and sonicated until a homogeneous solution was formed. Then, NiSO<sub>4</sub>·6H<sub>2</sub>O (0.2 g) was dissolved in 40 mL of water and added dropwise to the previous solution while stirring at ambient temperature for 5 h. After centrifuging at 10,000 rpm for 5 min, the precipitate was collected and rinsed several times with water. After lyophilization, the final product SPSDVB-PAA-Ni was acquired and kept for additional research.
- 2.4. Optimization of Protein Adsorption/Desorption Behaviors onto SPSDVB-PAA-Ni. The adsorption properties of SPSDVB-PAA-Ni were investigated using IgG, Trf, and BSA as representative model proteins. The stock protein solution was diluted with 40 mmol·L<sup>-1</sup> Britton-Robinson (B-R) buffer to obtain protein solutions with varying pH values and concentrations. The experiment procedure was executed as follows: the SPSDVB-PAA-Ni (2.0 mg) microparticles and protein solution (100  $\mu$ g·mL<sup>-1</sup>, 1 mL) at pH values spanning from 4.0 to 9.0 were mixed together in a centrifuge tube and oscillated for 30 min at ambient temperature. The supernatant was obtained via centrifugation at 6000 rpm for 5 min and then stained by Coomassie brilliant blue. The absorbance was measured at 595 nm, and the concentration of unabsorbed proteins was calculated by the standard working curve method. Equation 1 was used to calculate the efficiency of protein adsorption  $(E_1)$  in the experiment, where  $C_0$  and  $C_1$ represented the concentration of initial protein and residual protein, respectively.

$$E_1 = \frac{C_0 - C_1}{C_0} \times 100\% \tag{1}$$

After the supernatant was discarded, the precipitate was rinsed with B–R buffer and mixed with 1.0 mL of 0.1 wt % CTAB for 30 min to recover the adsorbed proteins on SPSDVB-PAA-Ni. After undergoing centrifugation and staining as previously described, the elution efficiency  $(E_2)$  was calculated by eq 2, where  $C_2$  represented the supernatant protein concentration after elution.

Scheme 1. Illustration for the Synthesis of SPSDVB-PAA-Ni and Selective Adsorption of IgG



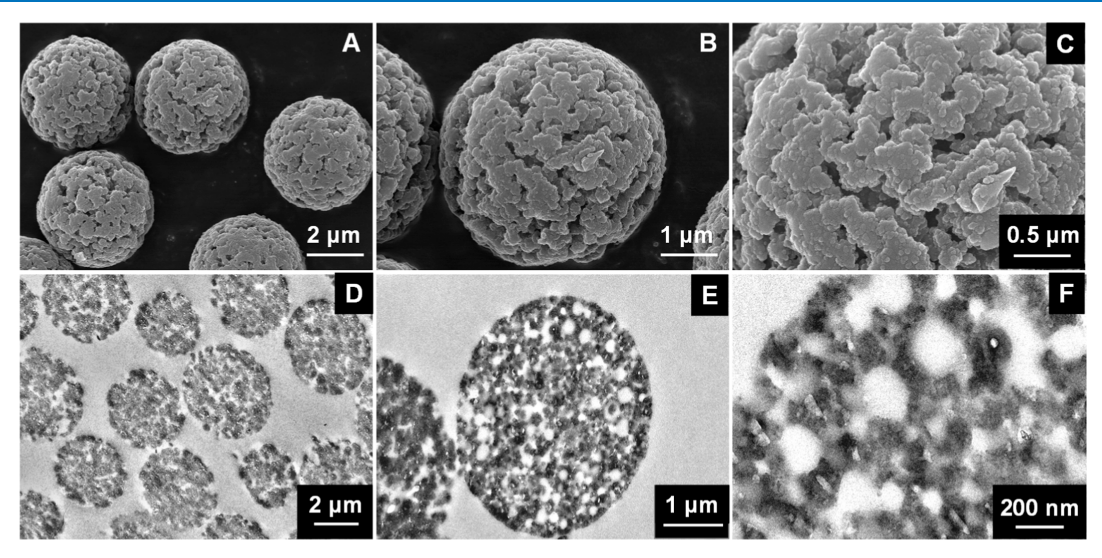


Figure 1. (A-C) SEM images of SPSDVB-PAA-Ni microparticles and (D-F) the cross-section TEM images of SPSDVB-PAA-Ni microparticles.

$$E_2 = \frac{C_2}{C_0 - C_1} \times 100\% \tag{2}$$

# 2.5. IgG Separation/Purification from Human Serum. Human serum was pretreated by diluting 100-fold with pH 6.0 B—R buffer and employed to test the practical utility of SPSDVB-PAA-Ni in purifying IgG from actual samples. The 100-fold diluted human serum sample (0.5 mL) was added to SPSDVB-PAA-Ni (5.0 mg). Following 30 min of shaking, the supernatant was obtained via centrifugation. Next, the precipitate was washed with pH 6.0 B—R buffer and mixed with 0.1 wt % CTAB (0.5 mL) as an eluent, followed by shaking for 30 min. Finally, the pretreated serum sample, the supernatant, and the eluent were collected and identified by SDS-PAGE. The purity and recovery of IgG from the human serum sample were calculated by eqs S1 and S2 given in the

# 3. RESULTS AND DISCUSSION

Supporting Information using ImageJ software.

**3.1.** Synthesis and Characterization of SPSDVB-PAA-Ni. The overview of the SPSDVB-PAA-Ni microparticle synthesis procedure is presented in Scheme 1. During the polymerization process in emulsion droplets, hydrophobic

monomers (styrene and divinylbenzene) and hydrophilic monomers (acrylic acid) initiated polymerization in the oil and water phases, respectively. Amphiphilic SPS particles could be a stabilizer for water-in-oil-in-water (W-in-O-in-W) emulsion interfaces. Then, the polymerization process occurred at both the oil-in-water external interface and the water-in-oil internal interface, resulting in the formation of hydrophilic—hydrophobic—hydrophilic heterostructure polymers. The polyacrylic acid layers on the surface and within the pores contained carboxyl groups, which were able to combine with nickel ions by means of electrostatic interaction. Finally, the nickel-functionalized porous heterostructure microparticles (SPSDVB-PAA-Ni) were produced and promoted the effective adsorption of IgG.

The surface morphologies of SPS and SPSDVB-PAA microparticles are shown in Figure S1. The SPS microspheres display a uniform size of  $2.09 \pm 0.06 \, \mu \text{m}$  with a smooth surface and good dispersion. Following emulsion polymerization, the size of SPSDVB-PAA microspheres increases to  $4.12 \pm 0.12 \, \mu \text{m}$ , and the surface takes on a rough texture covered with a large amount of dense pores. After functionalization with nickel ions, the size and morphology of SPSDVB-PAA-Ni, which are shown in Figure 1A–C, remain unchanged

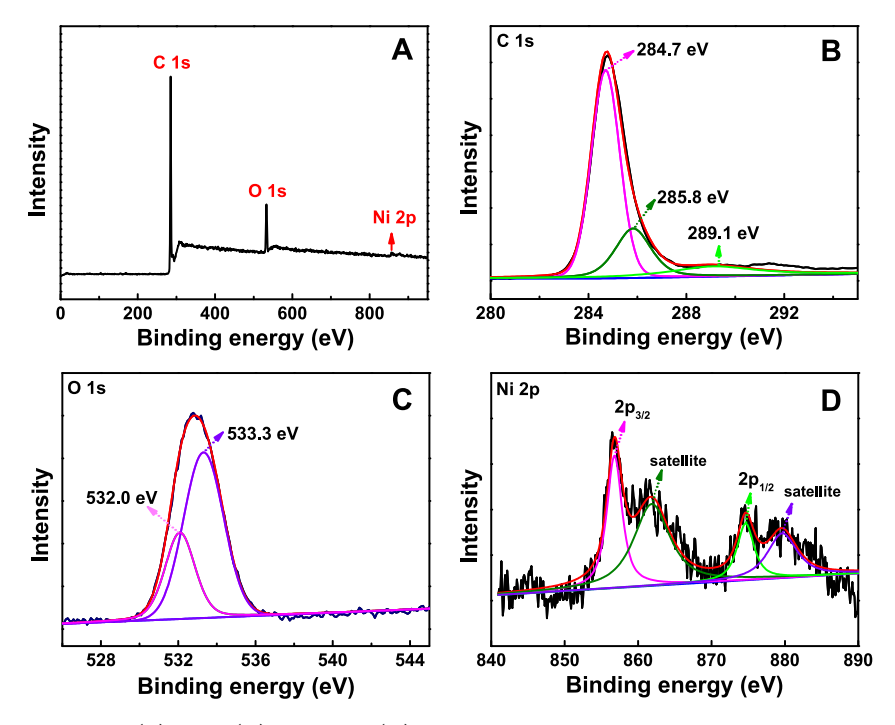


Figure 2. (A) XPS full spectrum and (B) C 1s, (C) O 1s, and (D) Ni 2p high-resolution XPS spectra of SPSDVB-PAA-Ni.

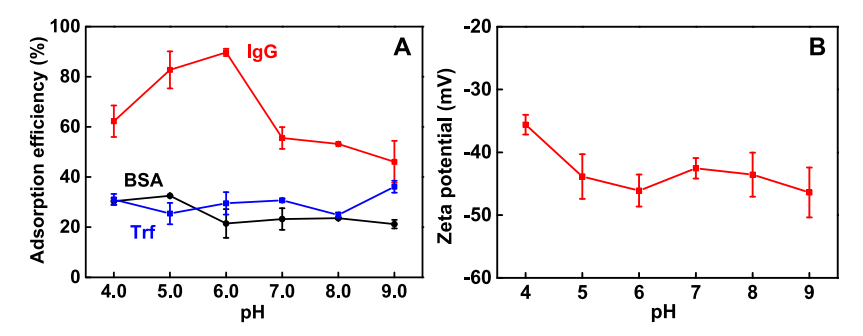


Figure 3. (A) pH-dependent adsorption efficiencies of IgG, BSA, and Trf by SPSDVB-PAA-Ni. Adsorbent mass: 2.0 mg; adsorption time: 30 min; protein solution: 100 μg·mL<sup>-1</sup>, 1.0 mL. (B) The zeta potentials of SPSDVB-PAA-Ni at pH 4–9.

compared to SPSDVB-PAA. This indicates that the introduction of nickel ions does not affect the porous structure and dispersibility of the microparticles. In Figure 1D—F, the cross-section TEM images exhibit an interior porous structure of SPSDVB-PAA-Ni. It is apparent that a substantial quantity of macropores is observed on both the outer surface and inside the microspheres. The presence of macropores in the microspheres is a promising feature that could greatly enhance their potential for protein adsorption.

The nitrogen adsorption—desorption experiment is performed to measure pore size distribution and specific surface area. The SPSDVB-PAA-Ni microparticles exhibit type III isotherm adsorption curves in Figure S2A, indicating irregular large pore structures. The Brunauer—Emmett—Teller (BET) surface area was determined to be 7.09 m² g⁻¹, and the pore size distribution diagram in Figure S2B reveals that the most probable pore size is around 60.9 nm by utilizing the Barret—Joyner—Halenda method. The large pores of SPSDVB-PAA-Ni enable protein molecules to penetrate the porous structure, increasing the quantity of recognition sites accessible for protein interaction.

The functional groups of SPSDVB-PAA-Ni are determined by the FTIR spectrum in Figure S3. The stretching vibrations of -CH= groups in the benzene ring are observed at 3081, 3058, and 3025 cm<sup>-1</sup>. The asymmetric and symmetric stretching vibrations of  $-\text{CH}_2-$  are indicated by the absorption peaks at 2921 and 2850 cm<sup>-1</sup>, respectively. The bending vibrations of the benzene ring C=C bonds can be seen at 1601, 1491, and 1449 cm<sup>-1</sup>. The characteristic absorption bonds of carboxyl groups (C=O) in polyacrylic acid are displayed at 1703 cm<sup>-1</sup>. These results demonstrate that the preparation of polymer microspheres containing polystyrene, polydivinylbenzene, and polyacrylic acid was successfully accomplished.

The XPS analysis is employed to characterize the chemical composition of SPSDVB-PAA-Ni. Analysis of the XPS spectrum of SPSDVB-PAA-Ni in Figure 2A demonstrates the presence of characteristic peaks for C 1s, O 1s, and Ni 2p, confirming that the SPSDVB-PAA-Ni microspheres consist of C, O, and Ni elements. The C 1s high-resolution XPS spectrum in Figure 2B exhibits three typical peaks at 284.7, 285.8, and 289.1 eV, assigned to the C-C=C, C-O, and C=O groups, respectively. In Figure 2C, the O 1s high-resolution XPS spectrum is deconvoluted into two peaks corresponding to C=O and C-O groups at 532.0 and 533.3 eV, respectively. These results imply that benzene rings and

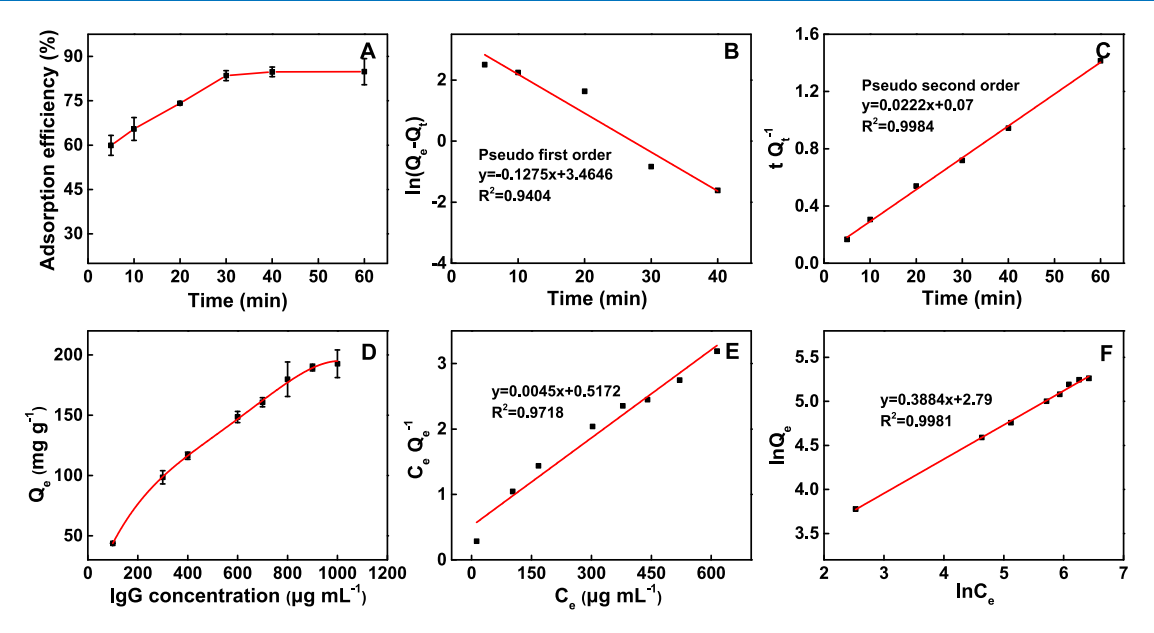


Figure 4. (A) Effect of adsorption time on the adsorption property of SPSDVB-PAA-Ni toward IgG. Adsorption kinetics curves fitted with (B) pseudo-first-order and (C) pseudo-second-order models. (D) Adsorption isotherms of IgG onto SPSDVB-PAA-Ni. (E) The Langmuir model fitting curve. (F) The Freundlich model fitting curve.

carboxyl groups are present in the SPSDVB-PAA-Ni compound. The Ni 2p XPS spectrum in Figure 2D reveals two peaks at 856.7 and 874.6 eV, identified as the Ni 2p<sub>3/2</sub> and Ni 2p<sub>1/2</sub>, respectively. The high-spin orbital peaks, along with two satellite peaks at 861.9 and 879.5 eV, indicate the existence of Ni<sup>2+</sup> on the surface of SPSDVB-PAA-Ni microsphere. In SPSDVB-PAA-Ni, the elemental distribution of C, O, and Ni is determined to be 87.4%, 12.0%, and 0.6%, respectively. It is evident from the above results that the polymer microspheres are synthesized and Ni<sup>2+</sup> is effectively modified on the surface of SPSDVB-PAA-Ni.

3.2. Protein Adsorption Behaviors onto SPSDVB-PAA-Ni. The isoelectric points (pI) of IgG, Trf, and BSA are 8.0, 5.4, and 4.9, respectively. The adsorption behaviors of three proteins onto SPSDVB-PAA-Ni microspheres are evaluated within a pH range of 4.0 to 9.0. As shown in Figure 3A, SPSDVB-PAA-Ni, as an adsorbent, exhibits higher adsorption efficiencies toward IgG than Trf and BSA at a wide pH range, suggesting specific interactions between SPSDVB-PAA-Ni and IgG. As anchor sites, Ni<sup>2+</sup> can coordinate to nitrogen atoms in the imidazole ring of histidine residues. Due to the existence of an accessible histidine cluster  $(pK_a = 6.04)$  in the IgG Fc fragment, the metal affinity interaction could occur between Ni2+ in SPSDVB-PAA-Ni and histidine residues in IgG. It is evident that exposed histidine residues display the highest affinity for metal ions.<sup>20</sup> Therefore, the pH values could affect the strength of the affinity interaction. At pH 6.0, histidine residues within the Fc domain are neutral and exposed on the surface of proteins, promoting a strong affinity interaction of the SPSDVB-PAA-Ni polymer microspheres to IgG. 36,37 When the pH is below or above 6.0, histidine residues are buried in the Fc domain, making it unfavorable for binding to the adsorbent.

Furthermore, the adsorption of IgG is significantly influenced by electrostatic interactions, which vary depending on the pH values. Surface charges of SPSDVB-PAA-Ni microspheres at pH 4.0–9.0 are shown in Figure 3B, and the results prove they are negatively charged. Zeta potential

measurements were conducted for SPSDVB-PAA-Ni before and after IgG adsorption at pH 6.0. The material exhibits a zeta potential of  $-46.10 \pm 2.55$  mV in the initial state, which significantly increases to  $-14.50 \pm 1.60$  mV after IgG adsorption. The potential shift confirms the occurrence of electrostatic attraction interactions between SPSDVB-PAA-Ni and IgG. When the pH level is below 8.0 (pI of IgG), positively charged IgG leads to electrostatic attraction interactions with negatively charged carboxylate groups in SPSDVB-PAA-Ni. Even though a lower pH value results in a stronger electrostatic attraction, the metal affinity interaction becomes weaker when the pH drops below 6.0 due to the existence of protonated histidine residues in the IgG Fc domain. Hence, the highest adsorption efficiency of SPSDVB-PAA-Ni to IgG is obtained at pH 6.0, based on the effects of metal affinity and electrostatic attraction interactions. By contrast, the adsorption efficiencies of BSA and Trf are less than 40% over a wide pH range. Since the pI values of BSA and Trf are approximately 5.0, they may carry negative net charges when the pH is above 5.0. As a result, there could be an electrostatic repulsion interaction between SPSDVB-PAA-Ni and BSA or Trf at pH 6.0 that contributes to reduced adsorption efficiencies. Therefore, the optimal pH for separation of IgG is 6.0, and this pH value has been selected for additional research.

In order to clarify the contribution of Ni<sup>2+</sup>, the adsorption experiment was conducted on SPSDVB-PAA microspheres without Ni<sup>2+</sup> for comparison with SPSDVB-PAA-Ni microspheres. The results are shown in Figure S4. At pH 6.0, the SPSDVB-PAA microspheres demonstrate higher adsorption efficiency toward IgG than BSA and Trf, which is attributed to electrostatic attraction between the negatively charged carboxylate groups in SPSDVB-PAA and positively charged IgG. Following Ni<sup>2+</sup> modification, the adsorption efficiency toward IgG increases from 75.8% to 89.7%, indicating that Ni<sup>2+</sup> enhances the selective adsorption of IgG via specific Ni<sup>2+</sup>-histidine residue affinity interaction.

Adsorption kinetics and adsorption isotherms play important roles in evaluating the adsorption equilibrium. Figure 4A

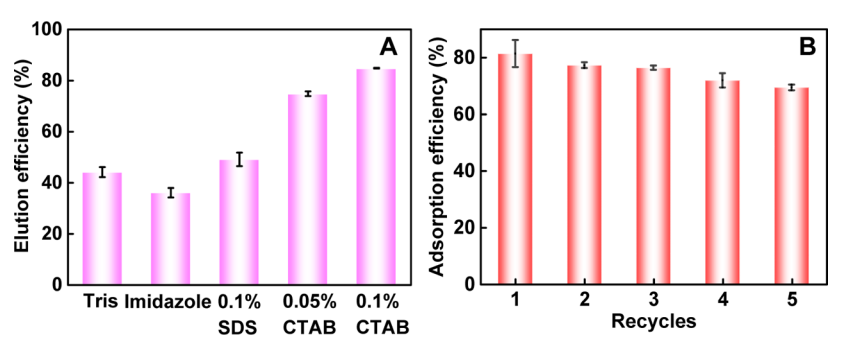


Figure 5. (A) The elution efficiencies of the captured IgG from SPSDVB-PAA-Ni by various elution reagents. (B) The adsorption efficiencies of SPSDVB-PAA-Ni for IgG over five adsorption—desorption cycles.

displays the time-dependent adsorption efficiencies of IgG onto SPSDVB-PAA-Ni at an IgG concentration of 100  $\mu$ g·mL<sup>-1</sup>. The adsorption efficiencies increase quickly and approach equilibrium within the initial 30 min, resulting in over 80% of IgG being captured onto SPSDVB-PAA-Ni. The high adsorption rates are attributed to abundant available recognizing sites exposed on the surface of SPSDVB-PAA-Ni with a nanoporous structure. Thus, adsorption time is maintained at 30 min in the following adsorption experiments. To investigate the adsorption mechanism, the adsorption kinetics data are fitted with the pseudo-first-order and pseudo-second-order kinetic models, as depicted in eqs 3 and 4:

$$ln(Q_e - Q_t) = ln Q_e - k_1 t \tag{3}$$

$$\frac{t}{Q_{t}} = \frac{1}{k_2 Q_{e}^2} + \frac{t}{Q_{e}} \tag{4}$$

where  $Q_{\rm e}$  (mg·g<sup>-1</sup>),  $Q_{\rm t}$  (mg·g<sup>-1</sup>), t (min),  $k_1$ , and  $k_2$  represent adsorption capacity at equilibrium and time t, adsorption time, the pseudo-first-order rate constant, and the pseudo-second-order rate constant, respectively. The fitted curves in Figures 4B and 4C and parameters in Table S1 indicate that the pseudo-second-order model is found to be more appropriate for the adsorption kinetics of IgG onto SPSDVB-PAA-Ni due to its higher correlation coefficient ( $R^2 = 0.9984$ ) and closer adsorption capacity. It is demonstrated that the adsorption process of SPSDVB-PAA-Ni to IgG is mainly governed by chemical adsorption.

To develop deeper into the binding properties, the adsorption isotherm of IgG is performed at room temperature, with protein concentrations ranging from 100 to 1000  $\mu$ g·mL<sup>-1</sup>. In Figure 4D, it is evident that the adsorption capacity of IgG increases as the initial concentration of IgG improves, reaching a maximum of 192.7 mg·g<sup>-1</sup>. The linearized Langmuir and Freundlich models expressed in eqs 5 and 6 are employed to fit the experimental values.

$$\frac{C_{\rm e}}{Q_{\rm e}} = \frac{C_{\rm e}}{Q_{\rm m}} + \frac{1}{K_{\rm L}Q_{\rm m}} \tag{5}$$

$$\ln Q_{\rm e} = \frac{1}{n} \ln C_{\rm e} + \ln K_{\rm F} \tag{6}$$

where  $C_{\rm e}$  ( $\mu{\rm g\cdot mL}^{-1}$ ),  $Q_{\rm e}$  ( $m{\rm g\cdot g}^{-1}$ ),  $Q_{\rm m}$  ( $m{\rm g\cdot g}^{-1}$ ),  $K_{\rm L}$ , and  $K_{\rm F}$  are the IgG free concentration at equilibrium, IgG equilibrium and maximum adsorption capacity, and Langmuir and Freundlich constants, respectively. 1/n represents the heterogeneity index. As shown in Figure 4E,F and Table S2, the Freundlich model ( $R^2 = 0.9981$ ) is a better fit compared to the

Langmuir model ( $R^2 = 0.9718$ ) based on the correlation coefficient  $R^2$ , indicating heterogeneous adsorption behavior of IgG onto SPSDVB-PAA-Ni. The Freundlich model displayed 1/n values below 1.0, suggesting favorable adsorption affinity of the sorbent toward IgG.<sup>38</sup>

**3.3. Protein Desorption Behaviors onto SPSDVB-PAA-Ni.** It is essential to retrieve the captured IgG on SPSDVB-PAA-Ni for further biological research. Tris (0.1 mol·L<sup>-1</sup>), imidazole (0.5 mol·L<sup>-1</sup>), 0.1 wt % SDS, 0.05 wt % CTAB, and 0.1 wt % CTAB are employed as stripping reagents to desorb IgG. As shown in Figure 5A, a satisfactory elution efficiency of 84.8% is provided by 0.1% CTAB in contrast to other reagents. The hydrophobic interactions between CTAB and IgG and the electrostatic attraction between cationic quaternary ammonium in CTAB and negatively charged SPSDVB-PAA-Ni facilitate the stripping of IgG from the surface of SPSDVB-PAA-Ni. Hence, 0.1 wt % CTAB solution is chosen as eluent for further investigations.

The regeneration performance of SPSDVB-PAA-Ni to IgG was assessed during five adsorption—desorption cycles, as illustrated in Figure 5B. The adsorption—elution cycles are maintained above 76% after three adsorption—elution cycles and decrease to 69.4% in the fifth cycle. To evaluate the stability of SPSDVB-PAA-Ni, the amounts of Ni<sup>2+</sup> in the eluent after the adsorption—desorption experiment were determined by ICP—MS analysis. The results show that the content of Ni<sup>2+</sup> is 9.38  $\mu$ g·L<sup>-1</sup> and 186.05  $\mu$ g·L<sup>-1</sup> in the first and fifth eluent, respectively. The slight loss of Ni<sup>2+</sup> causes reduced binding sites with IgG, leading to a decrease in adsorption efficiency.

3.4. Separation/Purification of IgG from Human Serum. The practical performance of SPSDVB-PAA-Ni in selectively separating IgG is evaluated using human serum as an actual biological sample. Diluted by 100-fold with pH 6.0 B-R, the human serum sample was processed through an adsorption-desorption procedure following the steps outlined in the Experimental Section. Figure 6 shows the SDS-PAGE assay results. The human serum sample is a complex matrix containing multiple protein bands in lane 1, mainly corresponding to Trf at 80 kDa, human serum albumin (HSA) at 66.4 kDa, IgG heavy chain at 50 kDa, and IgG light chain at 25 kDa. After treatment with SPSDVB-PAA-Ni, the supernatant in lane 2 exhibits less intense bands of IgG. Subsequently, the adsorbed proteins are eluted with 0.1 wt % CTAB, revealing two prominent protein bands at 50 and 25 kDa in lane 3, which match the standard IgG bands in lane 4. However, the eluent in lane 3 contains faint coadsorbed serum protein bands, such as HSA and Trf, which are attributed to nonspecific binding between these proteins and SPSDVB-

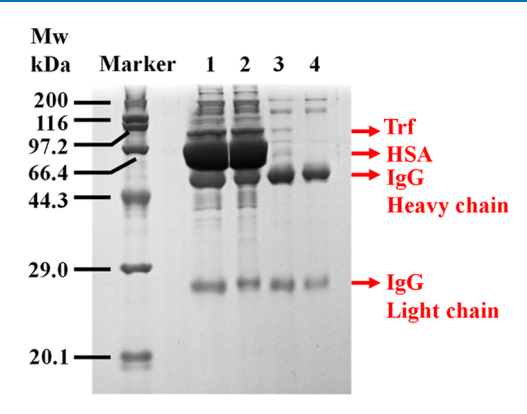


**Figure 6.** SDS-PAGE results. Marker: standard molecular weight (kDa); lane 1: 100-fold diluted human serum; lane 2: the supernatant of 100-fold diluted human serum after adsorption with SPSDVB-PAA-Ni; lane 3: the eluate recovered from SPSDVB-PAA-Ni; lane 4: IgG standard solution (100  $\mu$ g·mL<sup>-1</sup>).

PAA-Ni. The recovery and purity of IgG from human serum were 73.7% and 83.7% using SPSDVB-PAA-Ni. These results demonstrate that SPSDVB-PAA-Ni shows promise as an adsorbent for selectively isolating IgG from complicated biosamples.

The binding performance of SPSDVB-PAA-Ni toward IgG is further evaluated in comparison with the recently reported adsorbents, and the outcomes are presented in Table 1. The SPSDVB-PAA-Ni nanoporous microspheres exhibit higher adsorption capacity and shorter equilibrium time than other adsorbents, including protein A/G-Sepharose, <sup>39,40</sup> ABI-APBA/ FYE-ABI ligand-modified resins, 16,41 polyoxometalates, 33 metal-organic frameworks, 42,43 monolithic cryogels, 44 and polymers. 45 The exceptional binding performance of SPSDVB-PAA-Ni is attributed to its multimodal binding (metal affinity and electrostatic attraction interactions) and macroporous structure. Compared with protein A/G adsorbents, SPSDVB-PAA-Ni exhibits a slightly lower purity but significantly higher recovery. Due to the high cost and toxic ligand leakage of protein A/G adsorbents, SPSDVB-PAA-Ni has advantages of low cost, facile synthesis, and eco-friendly positioning, making it a promising alternative for IgG purification.

However, the purity and recovery of IgG are somewhat unsatisfactory. It is attributed to nonspecific adsorption of protein impurities in human serum, mainly HSA and Trf, with SPSDVB-PAA-Ni. In addition, the loss of Ni<sup>2+</sup> after several adsorption—elution cycles results in a reduced number of binding sites with IgG, leading to a decline in adsorption efficiency. Potential strategies could be employed in the future

to improve the binding performance of the material. First, introducing reagents with high grafting density to immobilize Ni<sup>2+</sup> on the polymer surface could enhance the Ni<sup>2+</sup> content while decreasing Ni<sup>2+</sup> leakage. Second, the surface of materials can be modified with hydrophilic molecules like polyethylene glycol (PEG) or zwitterionic polymers to decrease nonspecific adsorption of hydrophobic interactions. In addition, a deep analysis of proteomic research could strengthen the potential applications of the synthesized microspheres in clinical diagnosis.

### 4. CONCLUSIONS

In this work, a low-cost, easily prepared adsorbent is developed through the modification of nickel ions on the surface of nanoporous heterostructure microparticles produced via emulsion interfacial polymerization. The dense macroporous structures throughout the entire microsphere enable the adsorption of proteins. Given that there is a histidine cluster in the Fc region of IgG, SPSDVB-PAA-Ni can interact with IgG via metal affinity interaction and electrostatic attraction interactions. It has been demonstrated that SPSDVB-PAA-Ni has adsorption selectivity toward IgG and ensures effective separation/purification of IgG from complicated biological samples. This work is expected to provide a promising adsorbent for the thorough purification of antibody drugs, thereby enhancing their utilization in clinical analysis.

### ASSOCIATED CONTENT

# **Supporting Information**

The Supporting Information is available free of charge at https://pubs.acs.org/doi/10.1021/acsomega.5c04837.

Preparation of sulfonated polystyrene (SPS); preparation of heterostructure SPSDVB-PAA microparticles; equations of the purity and recovery of IgG from the human serum sample; SEM images of the SPS and SPSDVB-PAA microparticles; N<sub>2</sub> adsorption/desorption isotherms and pore size distributions of SPSDVB-PAA-Ni; FTIR spectrum of SPSDVB-PAA-Ni; adsorption efficiencies of IgG, BSA, and Trf on SPSDVB-PAA-Ni and SPSDVB-PAA microspheres; adsorption kinetics models and parameters of IgG adsorbed by SPSDVB-PAA-Ni; and Langmuir and Freundlich model parameters of IgG on SPSDVB-PAA-Ni (PDF)

### AUTHOR INFORMATION

# **Corresponding Author**

Mengmeng Wang — Shenyang Key Laboratory of Medical Molecular Theranostic Probes, School of Pharmacy, Shenyang

Table 1. Binding Performances of SPSDVB-PAA-Ni Microparticles Compared with Other Adsorbents

adsorbents	adsorption time (min)	adsorption capacity $(mg \cdot g^{-1})$	purity (%)	recovery (%)	refs
protein A-Sepharose		29.2 mg·mL <sup>-1</sup>	84.7	65.1	39
protein G-Sepharose		18.9 mg·mL <sup>-1</sup>	97.6	69.6	40
ABI-APBA resin	180	187.0	94.9	94.3	16
FYE-ABI resin	180	91.0	93.9	88.9	41
SPSDVB-PAA-PEI-P <sub>5</sub> W <sub>30</sub>	30	117.6			33
UiO@GO@PEG	30	139.6			42
Co-MOF-OH	30	158.0			43
PAAm-Alg-ECH-P-Tyr	120	91.8	95.0	63.0	44
PAMAM-PNIPAAm-MEP		145.7	98.0	90.0	45
SPSDVB-PAA-Ni	30	192.7	83.7	73.7	this work

Medical College, Shenyang 110034, China; oorcid.org/0000-0001-5517-2529; Phone: +86 24 62215711; Email: wangmengmeng@symc.edu.cn

### **Authors**

- Yang Zhang Shenyang Key Laboratory of Medical Molecular Theranostic Probes, School of Pharmacy, Shenyang Medical College, Shenyang 110034, China; ⊙ orcid.org/0000-0001-9594-1695
- Wanting Zhang Shenyang Key Laboratory of Medical Molecular Theranostic Probes, School of Pharmacy, Shenyang Medical College, Shenyang 110034, China
- Jin Li Shenyang Key Laboratory of Medical Molecular Theranostic Probes, School of Pharmacy, Shenyang Medical College, Shenyang 110034, China
- Jiaxin Han Shenyang Key Laboratory of Medical Molecular Theranostic Probes, School of Pharmacy, Shenyang Medical College, Shenyang 110034, China
- Xiangyang Gong Shenyang Key Laboratory of Medical Molecular Theranostic Probes, School of Pharmacy, Shenyang Medical College, Shenyang 110034, China

Complete contact information is available at: https://pubs.acs.org/10.1021/acsomega.5c04837

### **Author Contributions**

<sup>†</sup>Y.Z. and W.Z. contributed equally to this work.

### Notes

The authors declare no competing financial interest.

### ACKNOWLEDGMENTS

The authors appreciate financial support from the Shenyang Science and Technology Talent Special Project (RC230022) and Natural Science Foundation of Liaoning Province (2023-BSBA-299 and 2023-MSLH-294).

### REFERENCES

- (1) Seifert, M.; Küppers, R. Human memory B cells. *Leukemia* **2016**, 30, 2283–2292.
- (2) Wang, K.; Zhang, H.; Jin, N.; Zhou, Y.; Guo, X.; Zhong, W.; Li, X.; Li, X.; Zhang, Y. Interfacial modification of recombinant protein for immunoglobulin G adsorption with spindle-shaped MOF as nano molecular containers. *Talanta* **2024**, *280*, 126535.
- (3) Schroeder, H. W.; Cavacini, L. Structure and function of immunoglobulins. *J. Allergy Clin. Immunol.* **2010**, *125*, 41–52.
- (4) Chi, Z.; Wu, X.; Zhang, Q.; Zhai, F.; Xu, Z.; Zhang, D.; Chen, Q. Titanium-based metal-organic framework MIL-125(Ti) for the highly selective isolation and purification of immunoglobulin G from human serum. *J. Sep. Sci.* **2022**, *45*, 3754–3762.
- (5) Capela, E. V.; Bairos, J.; Pedro, A. Q.; Neves, M. C.; Raquel Aires-Barros, M.; Azevedo, A. M.; Coutinho, J. A. P.; Tavares, A. P. M.; Freire, M. G. Supported ionic liquids as customizable materials to purify immunoglobulin G. Sep. Purif. Technol. 2023, 305, 122464.
- (6) Daller, J. Biosimilars: A consideration of the regulations in the United States and European union. *Regul. Toxicol. Pharmacol.* **2016**, 76, 199–208.
- (7) Zhou, W. B.; Graner, M.; Beseler, C.; Domashevich, T.; Selva, S.; Webster, G.; Ledreux, A.; Zizzo, Z.; Lundt, M.; Alvarez, E.; Yu, X. L. Plasma IgG aggregates as biomarkers for multiple sclerosis. *Clin. Immunol.* **2023**, *256*, 109801.
- (8) Kdimati, S.; Mullins, C. S.; Linnebacher, M. Cancer-cell-derived IgG and its potential role in tumor development. *Int. J. Mol. Sci.* **2021**, 22, 11597.
- (9) Bourel, L.; Bray, F.; Vivier, S.; Flament, S.; Guilbert, L.; Chepy, A.; Rolando, C.; Launay, D.; Dubucquoi, S.; Sobanski, V. Comparative analysis of laboratory-scale immunoglobulin G purifica-

- tion methods from human serum. J. Proteome Res. 2024, 23, 3933-3943.
- (10) Hirano, A.; Kanoh, S.; Shiraki, K.; Wada, M.; Kitamura, M.; Kato, K. Selective and high-capacity binding of immunoglobulin G to zirconia nanoparticles modified with phosphate groups. *Colloids Surf., B* **2023**, 226, 113291.
- (11) Jing, S. Y.; Gou, J. X.; Gao, D.; Wang, H. B.; Yao, S. J.; Lin, D. Q. Separation of monoclonal antibody charge variants using cation exchange chromatography: resins and separation conditions optimization. Sep. Purif. Technol. 2020, 235, 116136.
- (12) Ghosh, R.; Wang, L. Purification of humanized monoclonal antibody by hydrophobic interaction membrane chromatography. *J. Chromatogr. A* **2006**, *1107*, 104–109.
- (13) Farzi-Khajeh, H.; Toraby, S.; Akbarzadeh-Khiavi, M.; Safary, A.; Somi, M. H. Development of biomimetic triazine-based affinity ligands for efficient immunoglobulin G purification from human and rabbit plasma. *J. Chromatogr. A* **2022**, *1684*, 463559.
- (14) Low, D.; O'Leary, R.; Pujar, N. S. Future of antibody purification. J. Chromatogr. B 2007, 848, 48-63.
- (15) Mazzer, A.; Perraud, X.; Halley, J.; O'Hara, J.; Bracewell, D. Protein A chromatography increases monoclonal antibody aggregation rate during subsequent low pH virus inactivation hold. *J. Chromatogr. A* **2015**, *1415*, 83–90.
- (16) Liu, X.; Niu, J.; Shen, J.; Chu, H.; Wang, C.; Wei, Y. Boronate affinity/hydrophobic charge induction synergistic adsorption for improving purification of antibody. *Chem. Eng. J.* **2024**, 483, 149216.
- (17) El Khoury, G.; Lowe, C. R. A biomimetic Protein G affinity adsorbent: an Ugi ligand for immunoglobulins and Fab fragments based on the third IgG-binding domain of protein G. *J. Mol. Recognit.* **2013**, *26*, 190–200.
- (18) Salha, D.; Andaç, M.; Denizli, A. Molecular docking of metal ion immobilized ligands to proteins in affinity chromatography. *J. Mol. Recognit.* **2020**, *34*, 2875.
- (19) Lingg, N.; Öhlknecht, C.; Fischer, A.; Mozgovicz, M.; Scharl, T.; Oostenbrink, C.; Jungbauer, A. Proteomics analysis of host cell proteins after immobilized metal affinity chromatography: Influence of ligand and metal ions. *J. Chromatogr. A* **2020**, *16*33, 461649.
- (20) Moore, C. P.; Pieterson, K.; DeSousa, J. M.; Toote, L. E.; Wright, D. W. Characterization and utility of immobilized metal affinity-functionalized cellulose membranes for point-of-care malaria diagnostics. *J. Chromatogr. B* **2021**, *1186*, 123023.
- (21) Xu, Q.; Jiang, W.; Bu, F.; Wang, Z. F.; Jiang, Y. Magnetic dendritic polymer nanospheres for high-performance separation of histidine-rich proteins. ACS Appl. Mater. Interfaces 2023, 15, 30837—30848
- (22) Ge, M.; Zhang, J.; Gai, Z.; Fan, R.; Hu, S.; Liu, G.; Cao, Y.; Du, X.; Shen, Y. Synthesis of magnetic Fe<sub>3</sub>O<sub>4</sub>@PS-ANTA-M<sup>2+</sup> (M = Ni, Co, Cu and Zn) nanospheres for specific isolation of histidine-tagged proteins. *Chem. Eng. J.* **2021**, *404*, 126427.
- (23) Shi, S.; Zhang, W.; Wu, H.; Li, Y.; Ren, X.; Li, M.; Liu, J.; Sun, J.; Yue, T.; Wang, J. In situ cascade derivation toward a hierarchical layered double hydroxide magnetic absorbent for high-performance protein separation. ACS Sustainable Chem. Eng. 2020, 8, 4966–4974.
- (24) Wang, W.; Zhou, F.; Cheng, X.; Su, Z.; Guo, H. High-efficiency Ni<sup>2+</sup>-NTA/PAA magnetic beads with specific separation on his-tagged protein. *IET Nanobiotechnol.* **2020**, *14*, 67–72.
- (25) Todorova-Balvay, D.; Pitiot, O.; Bourhim, M.; Srikrishnan, T.; Vijayalakshmi, M. Immobilized metal-ion affinity chromatography of human antibodies and their proteolytic fragments. *J. Chromatogr. B* **2004**, 808, 57–62.
- (26) Mourão, C. A.; Carmignotto, G. P.; Bueno, S. M. A. Separation of human IgG fragments using copper, nickel, zinc, and cobalt chelated to CM-Asp-agarose by positive and negative chromatography. *J. Chromatogr. B* **2016**, *1017*, 163–173.
- (27) Song, Y.; Wan, X.; Wang, S. Heterostructured microparticles: From emulsion interfacial polymerization to separation applications. *Acc. Mater. Res.* **2023**, *4*, 1033–1045.

- (28) Gokmen, M. T.; Du Prez, F. E. Porous polymer particles—A comprehensive guide to synthesis, characterization, functionalization and applications. *Prog. Polym. Sci.* **2012**, *37*, 365–405.
- (29) Song, Y.; Bao, H.; Shen, X.; Li, X.; Liang, X.; Wang, S. Emerging nanoporous materials for biomolecule separation. *Adv. Funct. Mater.* **2022**, 32, 2113153.
- (30) Song, Y.; Zhou, J.; Zhu, Z.; Li, X.; Zhang, Y.; Shen, X.; O'Reilly, P.; Li, X.; Liang, X.; Jiang, L.; et al. Heterostructure particles enable omnidispersible in water and oil towards organic dye recycle. *Nat. Commun.* **2023**, *14*, 5779.
- (31) Chern, C. S. Emulsion polymerization mechanisms and kinetics. *Prog. Polym. Sci.* **2006**, 31, 443–486.
- (32) Song, Y.; Fan, J. B.; Li, X.; Liang, X.; Wang, S. pH-regulated heterostructure porous particles enable similarly sized protein separation. *Adv. Mater.* **2019**, *31*, 1900391.
- (33) Wang, M. M.; Chen, S.; Yu, Y. L.; Wang, J. H. Polyoxometalate-functionalized macroporous microspheres for selective separation/enrichment of glycoproteins. *Chem. Commun.* **2020**, *56*, 9870–9873.
- (34) Liu, L.; Xie, K.; Wang, Y.; Wang, H.; Wang, J.; Zhuang, Y.; Zhang, Y. Polyhedral oligomeric silsesquioxane-modulated mesoporous amorphous bimetallic organic frameworks for the efficient isolation of immunoglobulin G. *Talanta* 2025, 282, 126949.
- (35) Chen, Q.; Zhang, L.; Zhang, Y.; Shen, J.; Zhang, D.; Wang, M. High-efficient depletion and separation of histidine-rich proteins via Cu<sup>2+</sup>-chelated porous polymer microspheres. *Talanta* **2024**, 277, 126337.
- (36) O'Brien, J.; Shea, K. J. Tuning the protein corona of hydrogel nanoparticles: The synthesis of abiotic protein and peptide affinity reagents. *Acc. Chem. Res.* **2016**, *49*, 1200–1210.
- (37) Lee, S.-H.; Hoshino, Y.; Randall, A.; Zeng, Z.; Baldi, P.; Doong, R.-A.; Shea, K. J. Engineered synthetic polymer nanoparticles as IgG affinity ligands. *J. Am. Chem. Soc.* **2012**, *134*, 15765–15772.
- (38) Liu, S.; Hu, Z.; Zhang, X.; Tang, N.; Ou, H.; Pan, J. Selective separation of target glycoproteins using boronate affinity imprinted copolymers: precise identification and increase the number of recognition sites. *Sep. Purif. Technol.* **2023**, 326, 124865.
- (39) Lund, L. N.; Gustavsson, P. E.; Michael, R.; Lindgren, J.; Nørskov-Lauritsen, L.; Lund, M.; Houen, G.; Staby, A.; St. Hilaire, P. M. Novel peptide ligand with high binding capacity for antibody purification. *J. Chromatogr. A* **2012**, *1225*, 158–167.
- (40) Wang, Z.; Liang, Q.; Wen, K.; Zhang, S.; Shen, J. Antibody purification using affinity chromatography: A case study with a monoclonal antibody to ractopamine. *J. Chromatogr. B* **2014**, *971*, 10–13.
- (41) Zou, X.; Zhang, Q.; Lu, H.; Lin, D.; Yao, S. Development of a hybrid biomimetic ligand with high selectivity and mild elution for antibody purification. *Chem. Eng. J.* **2019**, *368*, 678–686.
- (42) Hu, Z.; Wang, X.; Wang, J.; Chen, X. PEGylation of metalorganic framework for selective isolation of glycolprotein immuno-globulin G. *Talanta* **2020**, 208, 120433.
- (43) Hu, Z.; Meng, J.; Wang, X.; Li, W.; Chen, X. Tailoring the surface properties of co-based metal-organic frameworks for highly efficient and selective enrichment of immunoglobulin G. ACS Appl. Mater. Interfaces 2020, 12, 55453–55459.
- (44) Marcuz, C.; Alves Mourão, C.; Haupt, K.; Alves Bueno, S. M. Performance of phosphor-L-tyrosine immobilized onto alginate/polyacrylamide-based cryogels: effect of ligand coupling on human IgG adsorption and fab fragments separation. *J. Chromatogr. B* **2021**, *1165*, 122530.
- (45) Rahman, M.; Wang, J.; Xia, H.; Liu, J.; Bai, Q. High capacity temperature-responsive affinity chromatography designed for antibody separation. *Chem. Eng. J.* **2020**, *391*, 123561.



CAS BIOFINDER DISCOVERY PLATFORM™

# BRIDGE BIOLOGY AND CHEMISTRY FOR FASTER ANSWERS

Analyze target relationships, compound effects, and disease pathways

**Explore the platform** 

